Hydrogen Shuttle Relay via Ru-Cu dual sites for High-efficiency Nitrate Electroreduction to Green Ammonia

Heng Guo[abc*], Shiqi Tian[ab], Shumin Luo[ab], Haoran Wu[ab], Tingsong Li[ab], Guoxing Chen[d], Xin Tu[e], Weijun Tian[ab], Chun Tang[abc], Guidong Yang[f], Ying Zhou[ab*]

[a] *State Key Laboratory of Oil and Gas Reservoir Geology and Exploitation, Southwest Petroleum University, Chengdu, 610500, China*

[b] *School of New Energy and Materials, Southwest Petroleum University, Chengdu, 610500, China*

[c] *Sichuan-Chongqing Joint Key Laboratory of Green Hydrogen Production & Storage and Efficient Utilization, Southwest Petroleum University, Chengdu, 610500, China*

[d] *Department of Materials and Earth Sciences, Technical University Darmstadt, Peter-Grünberg-Str. 2, 64287 Darmstadt, Germany*

[e] *Department of Electrical Engineering and Electronics, University of Liverpool, Liverpool L69 3GJ, United Kingdom.*

[f] *XJTU-Oxford International Joint Research Laboratory of Catalysis, School of Chemical Engineering and Technology, Xi'an Jiaotong University, Xi'an, 710049, China*

*Corresponding author

Email addresses: heng.guo@swpu.edu.cn (Heng Guo), yzhou@swpu.edu.cn (Ying Zhou)

ABSTRACT: The electrocatalytic nitrate reduction reaction (NO_3^-RR) offers a promising pathway for green ammonia synthesis, yet suffers from inefficient hydrogen utilization due to competing proton consumption pathways. Here, we engineer a Ru-Cu_2O/Cu catalyst via cationic spatial confinement, where Ru incorporation induces a dynamic hydrogen shuttle relay between reaction active sites. In situ/operando characterization technologies and theoretical calculations reveal that Ru sites accelerate water dissociation kinetics, generating mobile H* species that shuttle between Ru and Cu_2O to synchronize dual reaction pathways: H*-mediated nitrate hydrogenation and electron-driven NH_x intermediate conversion. Crucially, this shuttle relay enables kinetic matching of H flux between NO_3^-RR and hydrogen evolution reaction, suppressing parasitic H_2 evolution while achieving a Faradaic efficiency (FE) of 95.68% with an NH_3 yield rate of 0.82 mmol cm^{-2} h^{-1} at -0.2 V vs. RHE—1.65-fold higher than Cu_2O/Cu controls. In addition, the catalyst maintains initial activity after 50 cycles. This work promotes the multi-step electrochemical hydrogenation process in nitrate reduction to ammonia (NO_3^-RR) by constructing an efficient hydrogen transport path.

Keywords: Electrocatalysis, Nitrate reduction, Hydrogen shuttle, Ru-Cu_2O/Cu, Ammonia

1. Introduction

Ammonia (NH_3), a crucial chemical feedstock in modern industry and agriculture, is gaining recognition as a carbon-neutral energy carrier due to its high hydrogen content. (17.6 wt%)[1–3]. The conventional Haber-Bosch (H-B) process, while indispensable historically, accounts for 1-2% of global energy consumption and contributes 450 million tons of annual CO_2-equivalent emissions, urgently requiring sustainable alternatives[4–6]. Electrocatalytic nitrogen reduction (NRR) presents theoretical promise but faces practical limitations, including limited N_2 solubility (0.02 g/L in water), which poses a severe engineering challenge for NRR. Even on the surface of active catalysts, the concentration of reactants is extremely low, thereby severely restricting the overall ammonia production rate and the formidable N≡N bond dissociation energy (~941 $kJ \cdot mol^{-1}$), results in the reaction requiring a very high overpotential to drive the initial N_2 activation, which significantly reduces energy efficiency and limits the reaction rate.[7–11]. Comparatively, electrocatalytic nitrate reduction (NO_3^-RR) demonstrates superior engineering prospects owing to nitrate's high aqueous solubility (880 g/L), enabling high reaction rates that are favorable for continuous flow scale-up production. Meanwhile, the lower N=O bond energy (204 kJ/mol) endows NO_3^-RR with faster reaction kinetics and higher potential energy efficiency, showing more superior engineering prospects.[7,12,13]. This approach simultaneously addresses nitrate pollution remediation and NH_3 synthesis, representing a dual-function environmental strategy[14–16]. However, the complex nine-proton-coupled eight-electron transfer pathway compromises its efficiency, competitive hydrogen evolution reactions, and incomplete conversion of intermediates (e.g., nitrite, NO), necessitating advanced electrocatalysts to enhance NH_3 selectivity and suppress byproducts[12,17].

In recent years, copper (Cu) has risen as a premier electrocatalyst for nitrate-to-ammonia conversion due to synergistic economic and electronic merits[18,19]. Its d-band center position closely aligns with nitrate's π* antibonding orbitals, enabling selective NO_3^- adsorption and efficient electron transfer during the rate-limiting $NO_3^- \rightarrow NO_2^-$ step[20–22]. Strategic material designs-alloying (e.g., $Cu_{50}Ni_{50}$ with 6×activity enhancement via optimized $^*NO_2$ binding)[23] and defect engineering transforms CuO nanosheets (CuO NPs) into defect-rich Cu nanosheets (dr-Cu NPs) through in situ electrochemical reduction, which enhances the adsorption of NO_3^- and related intermediates on the electrocatalyst surface, demonstrating tunable intermediate adsorption landscapes[24–27]. However, proton transfer limitations at Cu active sites impede critical $^*NH_x$ hydrogenation steps, constraining NH_3 yield below thermodynamic predictions. Therefore, in the design of catalysts, it is necessary to combine efficient adsorption sites for nitrate with the promotion of active hydrogen supply to overcome the kinetic limitations of the protonation step[28,29].

The decomposition of H_2O serves as the primary source of reactive hydrogen species (H*), making optimization of the volmer step crucial for enhancing the system's catalytic performance. In electrochemical nitrate reduction, effective H* supply enhancement must be strategically coupled with hydrogen evolution reaction (HER) suppression, necessitating catalysts with balanced hydrogen adsorption/desorption characteristics[30–32]. Notably, ruthenium (Ru) exhibits distinct advantages over conventional noble metals (Pd, Au, Pt, Rh, and Ir), combining relatively low cost with superior theoretical performance metrics[33–35]. Computational studies reveal Ru's lower overpotential than Pt and Pd counterparts, while its apex position on the ammonia synthesis volcano plot confirms exceptional catalytic efficiency[36]. Mechanistically, Ru facilitates both nitrogen dissociation activation and H* generation kinetics, enabling high NH_3 yield and selectivity under mild conditions. Importantly, dispersing Ru nanoparticles on high-surface-area carriers significantly reduces material costs while improving catalytic activity[32,37,38]. Thus, Ru-modified Cu_2O can promote water dissociation, potentially supplying more H* to enhance nitrate reduction activity.

Herein, we demonstrated a rationally designed Ru-Cu_2O/Cu (Ru-Cu_2O/Cu foam) electrocatalyst synthesized via controlled cation-exchange, achieving efficient nitrate-to-ammonia conversion. This architecture leverages redox interactions between Ru^{3+} and $Cu(OH)_2$/Cu ($Cu(OH)_2$/Cu foam) during synthesis, simultaneously generating Cu_2O domains and establishing electron highways for rapid charge transfer. The optimized catalyst exhibits exceptional performance with 95.68% Faradaic efficiency (FE) and 0.82 mmol cm^{-2} h^{-1} NH_3 yield at -0.2 V vs. RHE. By combining with electron spin resonance, in situ attenuated total reflection-surface enhanced infrared absorption spectroscopy, and density functional theory calculations, we confirmed that Ru-activated H_2O dissociation initiates hydrogen shuttle relay, where Cu_2O mediates directional H* transfer while maintaining selective NO_3^- chemisorption. Our findings establish a hydrogen shuttle relay mechanism for developing multifunctional electrocatalysts in sustainable nitrogen valorization systems.

2. Experimental

2.1. Synthesis of Cu_2O/Cu

A 1.5 mm-thick copper foam (Cu foam) was ultrasonically cleaned in ethanol, 1 M HCl, and ultrapure water for 10 min each to remove surface impurities. Subsequently, 0.114 g of ammonium persulfate and 0.5 g of sodium hydroxide were dissolved in 5 mL of ultrapure water. The Cu foam was immersed in this solution for 20 min to grow blue $Cu(OH)_2/Cu$ nanowires. The blue product was washed several times with ethanol and ultrapure water, followed by overnight drying in a vacuum oven. The $Cu(OH)_2/Cu$ nanowires were then annealed in a muffle furnace at 200 °C for 3 h with a heating rate of 2°C/min. The precursor was subsequently electrochemically activated via cyclic voltammetric pre-reduction in 0.1 M $KHCO_3$ electrolyte, scanning between -0.2 V and 0.2 V vs. RHE (Hg/HgO reference) at 5 mV/s for 10 cycles. The final catalyst was thoroughly washed with deionized water and ethanol, vacuum-dried for 1 h, and sectioned into 1×1 cm^2 working electrodes for subsequent testing.

2.2. Synthesis of Ru-Cu_2O/Cu

The copper foam substrate underwent sequential ultrasonic cleaning in ethanol, 1 M HCl, and ultrapure water (10 min each) to remove surface oxides. An aqueous solution containing 0.114 g ammonium persulfate and 0.5 g NaOH in 5 mL ultrapure water was prepared for nanowire growth. Immersion of the pretreated Cu foam in this oxidative alkaline solution for 20 min yielded vertically aligned $Cu(OH)_2$ nanowire arrays. After thorough rinsing with ethanol/water (3 cycles) and vacuum drying (60 °C, 12 h), the intermediate product was subjected to Ru incorporation via wet impregnation in 30 mL

$RuCl_3$ solution under continuous stirring (2 h). The Ru-functionalized precursor was subsequently washed, dried, and thermally converted to Ru-Cu_2O/Cu foam through controlled annealing (200 °C, 2 °C/min, 3 h). Electrochemical activation was performed by cyclic voltammetry in 0.1 M $KHCO_3$ (-0.2 to 0.2 V vs. RHE, Hg/HgO reference) at 5 mV/s for 10 cycles. The resulting catalyst was rinsed with deionized solvents, vacuum-dried (1 h), and tailored into 1×1 cm^2 working electrodes. A series of $RuCl_3 \cdot xH_2O$ solutions with varying concentrations were used to prepare precursors for Ru-Cu_2O/Cu with different Ru loadings, which were named 2 mM Ru-Cu_2O/Cu, 30 mM Ru-Cu_2O/Cu, and 50 mM Ru-Cu_2O/Cu (Ru-Cu_2O/Cu—Subsequent conclusions analysis is represented using this definition), respectively.

2.3. Electrochemical nitrate reduction measurements

All electrochemical tests were performed using an electrochemical workstation. (CHI760, Shanghai Chenhua). A three-electrode system was utilized, featuring Ru-Cu_2O/Cu and Cu_2O/Cu as working electrodes, a platinum sheet as the counter electrode, and an Hg/HgO electrode as the reference electrode. The electrolyte was 1 M KOH + 0.1 M KNO_3. All potentials were reported relative to the reversible hydrogen electrode (RHE) voltage ($E_{\mathrm{RHE}} = E_{\mathrm{Hg/HgO}} + 0.921$ V). Data were collected via linear sweep voltammetry (LSV) curves at a scan rate of 10 mV s^{-1}. The electrochemical active surface area (ECSA) was determined through cyclic voltammetry (CV) tests at various scan rates within the non-Faradaic potential range. Impedance spectra were obtained using electrochemical impedance spectroscopy (EIS) over a frequency range of 10^5 Hz to 0.1 Hz. The solution's reduced products were analyzed with a UV-Vis spectrophotometer (UV-2600, Shimadzu). All experiments took place under standard temperature and pressure conditions. Detailed materials synthesis protocols, characterization methods (XRD, XPS, TEM), *in-situ* ATR-SEIRAS configurations, and DFT computational parameters are provided in Supporting Information.

3. Results and discussion

3.1. Synthesis and characterization

The Ru-Cu_2O/Cu catalyst was fabricated through a three-step cation exchange protocol on Cu foam substrates. Initially, vertically aligned $Cu(OH)_2$ nanowires were hydrothermally grown on the Cu framework. Subsequently, controlled Ru deposition was achieved via immersion in $RuCl_3$ solutions with varying concentrations, followed by thermal annealing to yield the final Ru-Cu_2O/Cu architecture (Fig. 1a). As comparison, Cu_2O/Cu were also synthesized under the same conditions. The morphological evolution of catalyst architectures was systematically investigated through scanning electron microscopy (SEM). Comparative analysis reveals distinct structural differences between Cu_2O/Cu and Ru-Cu_2O/Cu. The pristine Cu_2O/Cu features three-dimensional nanowire arrays (NWAs) with hierarchical porosity, where interconnected macropores enable efficient electrolyte percolation while maximizing accessible active sites for nitrate electroreduction (Fig. S1-2). Upon Ru incorporation, octahedral Cu_2O nanoparticles exhibit Ru-content-dependent surface smoothing and dimensional expansion (Fig. S3-5 and 1b-d), suggesting enhanced metallic conductivity without compromising the structural integrity of the underlying NW substrate. Moreover, complementary transmission electron microscopy (TEM) analysis reveals critical structural insights into the Ru-Cu_2O/Cu catalyst. Low-magnification TEM images (Fig. S6) demonstrate conformal growth of a nanocrystalline rough layer on the Cu foam scaffold, confirming successful formation of the catalytic active layer. Atomic-resolution HRTEM imaging (Fig. 1e-g) combined with Fast Fourier transform (FFT)-derived SAED patterns identifies two distinct crystalline phases: single-crystalline Cu_2O domains with characteristic (111) and (200) lattice spacings of 0.245 nm and 0.212 nm, respectively, coexisting with metallic Cu crystallites (d_{220} = 0.127 nm)[39]. This phase coexistence corroborates partial substrate oxidation during synthesis. In addition, elemental mapping (Fig. S7) coupled with EDX spectroscopy (Fig. 1h-l) verifies Ru dispersion within the Cu_2O matrix[40], with spatially correlated Ru-Cu distributions that underpin the hydrogen shuttle functionality.

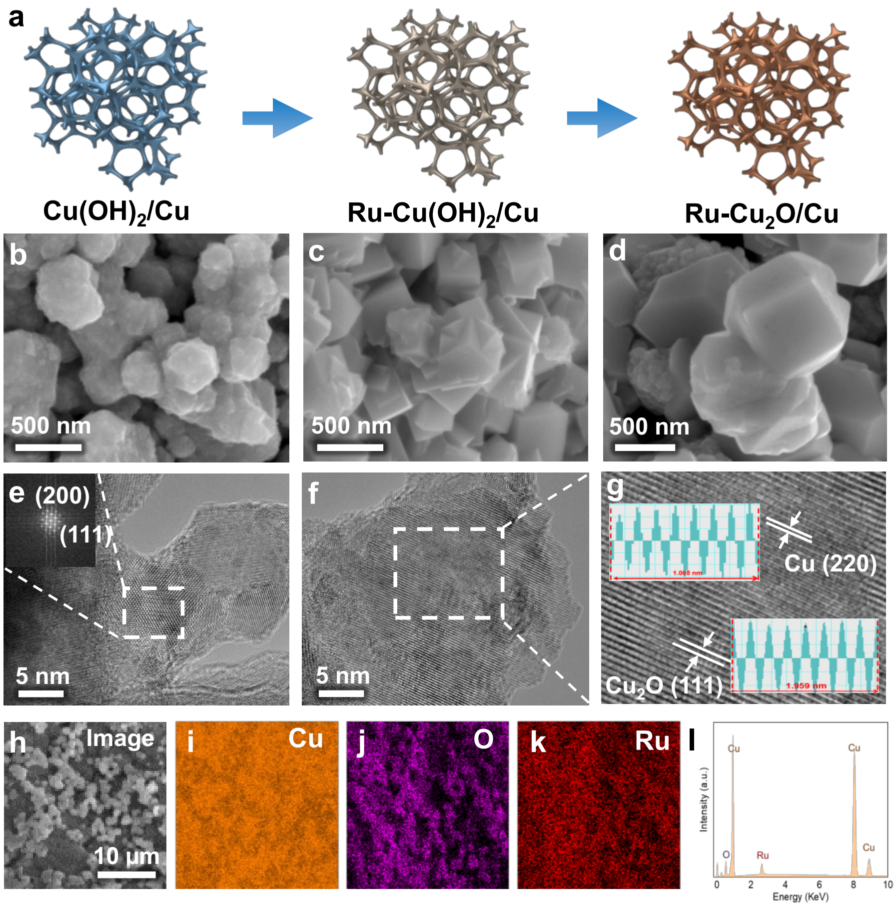

Fig. 1. (a) Schematic representation of the synthesis process for Ru-Cu_2O/Cu; (b, c) SEM images of 2 mM Ru-Cu_2O/Cu, 30 mM Ru-Cu_2O/Cu and (d) 50 mM Ru-Cu_2O/Cu; (e, g) HAADF-STEM image of Ru-Cu_2O/Cu; (h) Energy dispersive spectroscopy (EDS) elemental mapping of Ru-Cu_2O/Cu; (i) Cu; (j) O; (k) Ru; and (l) EDX spectrum of Ru-Cu_2O/Cu.

Structural characterization by X-ray diffraction (XRD) revealed distinct phase composition. As shown in Fig. 2a, the diffraction pattern exhibits precise alignment with standard cubic Cu (PDF#01-1242)[41] and cuprite Cu_2O (PDF#74-1230)[42]. Specifically, reflections at 36.3°, 42.6°, and 61.8° correspond to the (111), (200), and (220) crystallographic planes of Cu_2O, whereas peaks at 43.5°, 50.7°, and 74.7° originate from metallic Cu. The absence of Ru/RuO_2 diffraction peaks, consistent with previous reports[43], confirms Ru dispersion without the formation of detectable crystalline domains. Complementary Raman analysis (Fig. 2b) identified characteristic Cu_2O vibrational modes at 147, 218, 416, 515, and 634 cm^{-1}, alongside a weak CuO signal at 292 cm^{-1} [44,45], implying that Ru incorporation not only promotes Cu_2O formation but also induces partial Cu^+ oxidation to Cu^{2+} species.

To clarify the surface electronic structure of the Ru-Cu_2O/Cu catalyst, a systematic X-ray photoelectron spectroscopy (XPS) analysis was performed. The survey spectrum (Fig. S8) confirms predominant Cu and O signals with attenuated Ru intensity, consistent with its low surface concentration (0.53 at%) determined through elemental quantification (Cu: 44.31%, C: 26.93%, O: 28.22%). High-resolution Ru 3p spectra (Fig. 2c) reveal a characteristic spin-orbit doublet at 486.82 eV[40], corresponding to oxidized $Ru^{\delta+}$ species. As shown in Fig. 2d, the XPS spectrum of Cu 2p can be deconvoluted into spin-orbit peaks and satellite peaks. The peaks at 932.78 eV and 952.66 eV are attributed to Cu^{+}, which is consistent with the result from the Cu LMM Auger spectrum (Fig. S9), where the peak at 916.96 eV indicates that the Cu species in Ru-Cu_2O/Cu are in the oxidation state +1, while the peaks at 933.82 eV and 953.19 eV are attributed to Cu^{2+}[46–49]. Notably, the Cu 2p peak intensity in Ru-Cu_2O/Cu exhibits 1.5-fold enhancement versus Cu_2O/Cu, corroborating Raman observations of Ru-induced Cu_2O formation. A significant 0.32-0.38 eV positive shift in Cu 2p binding energies further confirms electron transfer from Cu to Ru atoms[47]. Complementary O 1s analysis (Fig. S10) identifies dual contributions from lattice oxygen (530.73 eV) and oxygen vacancies (531.92 eV)[50], collectively verifying the successful construction of Ru-Cu_2O interfaces with modulated electronic environments. Additionally, X-ray absorption fine structure (XAFS) spectroscopy was used to clarify the electronic configuration of Ru-Cu_2O/Cu. The Cu K-edge XANES spectra (Fig. 2e) display an intermediate absorption edge profile between Cu^{0} and Cu^{2+} standards. Then, Ru K-edge analysis (Fig. 2f) reveals mixed valence states spanning Ru^{0} to Ru^{4+}, demonstrating that Ru incorporation induces charge redistribution within the Cu_2O matrix[51]. This electronic interplay aligns with prior XPS analysis. Moreover, EXAFS analysis provides definitive structural evidence. The fitting results (Fig. S11-S12 and Table S1) confirm the presence of a ruthenium-oxygen coordination shell in the ruthenium K-edge spectrum, with a Ru-O coordination number of 4 and a bond length of 1.94 Å. Crucially, no ruthenium-ruthenium scattering paths were detected. The absence of such

Ru-Ru bonds clearly indicates that the ruthenium species exist predominantly as highly dispersed single atoms in the catalyst structure[52,53].

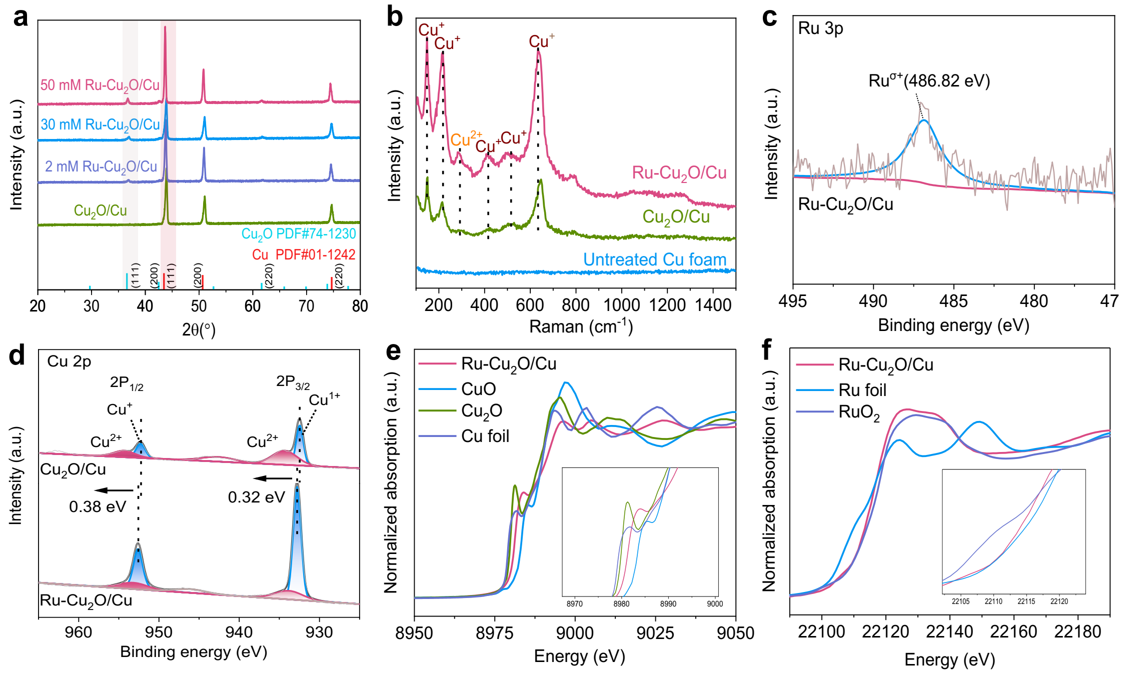

Fig. 2. (a) XRD diffraction patterns of Ru-Cu_2O/Cu; (b) Raman spectra of Ru-Cu_2O/Cu; (c) Ru 3p spectrum of Ru-Cu_2O/Cu; (d) Cu 2p spectrum of Ru-Cu_2O/Cu; (e) Cu K-edge XANES profiles of the Cu foil, Cu_2O, CuO, and Ru-Cu_2O/Cu; (f) Ru K-edge XANES profiles of the Ru foil, RuO_2, and Ru-Cu_2O/Cu.

3.2. Electrocatalytic performance

To investigate the activity and selectivity for ammonia synthesis from the nitrate reduction reaction (NO_3^-RR). The hierarchical nanoarchitecture of Ru-Cu_2O/Cu was subjected to systematic electrochemical evaluation in an H-cell with 1 M KOH + 0.1 M KNO_3 electrolyte. Quantitative analysis of ammonia production via chronoamperometry (0.5 h electrolysis, Fig. S13-16) demonstrates a Ru-content-dependent enhancement in nitrate-to-ammonia conversion. Fig. S17 shows that the 50 mM Ru-loaded (Ru-Cu_2O/Cu) catalyst achieves the highest ammonia yields and Faradaic efficiency compared to the other two electrocatalysts across all applied potentials from 0 to -0.4 V (vs. RHE). Subsequent investigations focused on this optimal Ru loading (50 mM), employing comprehensive electrochemical characterization to elucidate operational stability under continuous nitrate reduction conditions. A systematic evaluation of Ru-mediated electrocatalytic enhancement was conducted through linear sweep voltammetry (LSV) analysis.

As shown in Fig. 3a, their current densities increase after adding nitrate. With 0.1 M NO_3^- electrolyte, the current density increments for Ru-Cu_2O/Cu is significantly higher than for Cu_2O/Cu. For instance, at -0.2 V vs. RHE, the current density of Ru-Cu_2O/Cu rises by 42.8 mA cm^{-2} in the presence of nitrate, confirming the enhancement due to Ru-induced electronic structure. Notably, under operando conditions (-0.2 V vs. RHE), Ru-Cu_2O/Cu achieves record-breaking performance with 95.68% of FE and 0.82 mmol cm^{-2} h^{-1} of NH_3 yield rate (Fig. 3b-c), surpassing the control sample (84.6% FE, 0.50 mmol cm^{-2} h^{-1}) by 11.1% in FE and a 64% enhancement in NH_3 yield rate. During NO_3^-RR, NO_2^- is generated as a minor by-product and can be efficiently converted to ammonia. At -0.2 V vs. RHE, FE for nitrite byproducts is suppressed to 5.2% (Fig. 3d), in stark contrast to 19.2% observed for Cu_2O/Cu, indicating accelerated NO_2^- conversion kinetics. This reduction in intermediate accumulation correlates with enhanced NH_3 selectivity (Fig. 3e), where time-dependent concentration profiles (Fig. 3f) reveal NH_3 production dominates with minimal NO_2^- accumulation. Control experiments reveal minimal nonspecific NH_3 production (less than 0.822 mmol cm^{-2} h^-

^{1} in nitrate-free electrolyte; Fig. 3g), confirming that nitrate reduction to ammonia exhibits good selectivity.

To assess operational robustness under nitrate electroreduction conditions, Ru-Cu_2O/Cu catalyst underwent ten consecutive cycles at -0.2 V vs. RHE. Chronoamperometric profiles (Fig. S18) exhibit current density minor fluctuation with nearly superimposable UV-vis absorption curves, demonstrating exceptional cycle-to-cycle reproducibility. Furthermore, the Ru-Cu_2O/Cu catalyst maintained stable performance during the 84-hour extended stability test (Fig. S19). Quantitative analysis reveals minimal decay in NH_3 yield and FE (Fig. 3h), confirming the outstanding electrochemical durability. Additionally, post-catalysis characterization via XRD and XPS (Fig. S20-S23) shows retention of pristine crystallographic features Cu_2O (111). In terms of Faradaic efficiency, benchmarking against state-of-the-art catalysts (Fig. 3i and Table S2) shows Ru-Cu_2O/Cu achieves record-low potential (-0.2 V vs. RHE) while maintaining FE>95%. This catalyst significantly outperforms other recently reported electrocatalysts. Particularly at identical applied potentials, it exhibits higher FE, demonstrating promising application prospects[7,9,13,18,54–62].

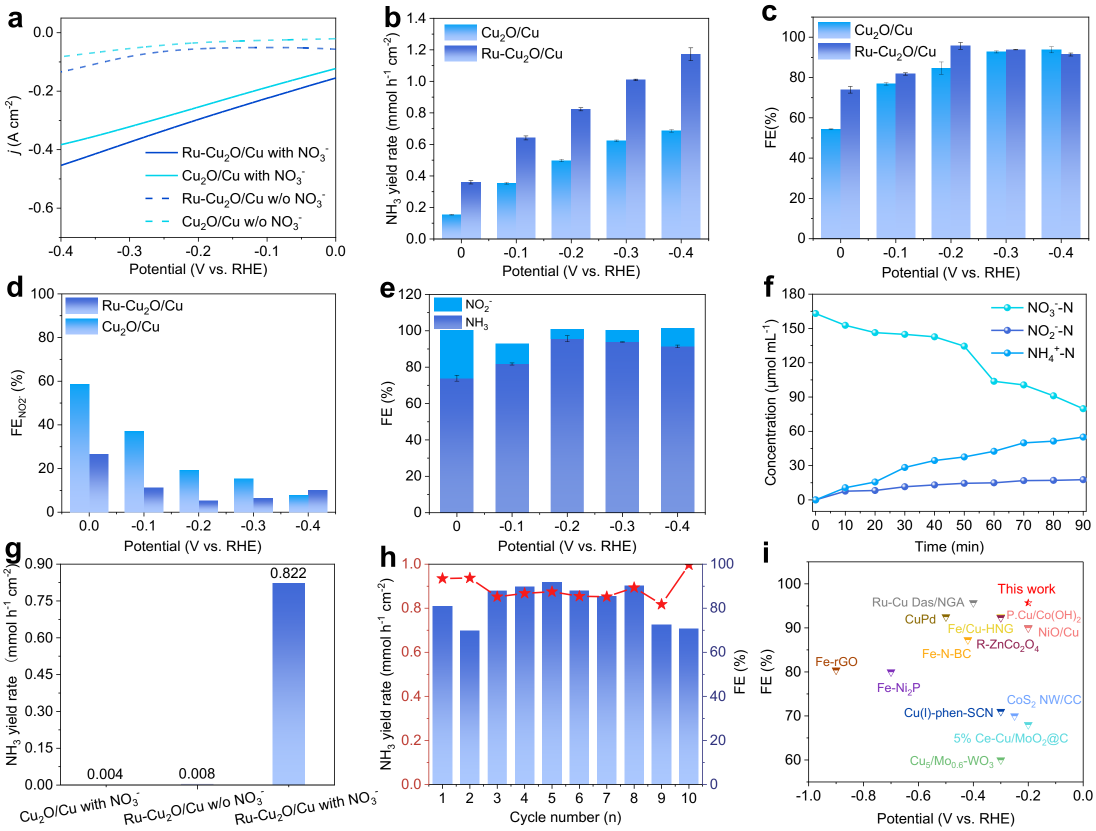

Fig. 3. Performance tests for electrochemical ammonia production. (a) LSV plots of Ru-Cu_2O/Cu versus Cu_2O/Cu with and without (w/o) nitrate; (b) NH_3 yield rates of Ru-Cu_2O/Cu versus Cu_2O/Cu and (c) Faraday efficiency; (d) NO_2^- Faraday efficiency of Ru-Cu_2O/Cu versus Cu_2O/Cu; (e) The product distribution for eNO_3RR on Ru-Cu_2O/Cu; (f) Time-dependent concentrations of NO_3^-, NO_2^-, and NO_4^+ over Ru-Cu_2O/Cu; (g) Control tests of Ru-Cu_2O/Cu; (h) NH_3 yield rates and FEs of Ru-Cu_2O/Cu during the recycling tests; (i) Comparison of FEs between Ru-Cu_2O/Cu and reported electrocatalysts.

3.3. Electrocatalytic activity analysis and mechanism investigation

To decipher the atomic-scale origin of the enhanced nitrate electroreduction activity, we systematically investigated the charge dynamics of Cu_2O/Cu-based catalysts. Cyclic voltammetry analysis in the non-Faradaic region (0.66-0.76 V vs RHE) with scan rates of 5-50 mV s^{-1} (Fig. S24) reveals a reduction in double-layer capacitance (C_{dl} = 0.022 mF cm^{-2}) compared to Cu_2O/Cu (0.137 mF cm^{-2}, Fig. 4a), demonstrating that activity enhancement stems from intrinsic activity rather than active site proliferation. Complementary EIS analysis (Fig. 4b) shows Ru-Cu_2O/Cu achieves lower charge transfer resistance. It can be deduced that the introduction of ruthenium enables accelerated hydrogen shuttling kinetics, contributing to the enhanced NO_3^-RR activity of Ru-Cu_2O/Cu. Contemporary mechanistic investigations have established the co-existence of dual pathways in nitrate electroreduction: direct electron transfer and hydrogen radical (H*)-mediated indirect reduction[63–66]. To probe the hydrogen shuttle dynamics in Ru-Cu_2O/Cu, we used electron spin resonance (ESR) spectroscopy with 5,5-dimethyl-1-pyrroline N-oxide (DMPO) as the spin-trapping agent. The distinct 1:2:2:1 quartet signal of DMPO-H* adducts (Fig. 4c-d and Fig. S25) demonstrates significant H* generation, with Ru-modified catalysts exhibiting higher signal intensity than Cu_2O/Cu in nitrate-free electrolyte, confirming Ru's catalytic superiority in H* evolution[67]. Complete signal attenuation during NO_3^-electrolysis validates rapid H* consumption through hydrogenation steps[68]. Notably, under nitrate-containing conditions, experimental validation of the Ru-Cu_2O/Cu catalyst during the 0-4 min testing period revealed stable surface H* signals, demonstrating the establishment of an efficient H* adsorption-desorption cycling mechanism. This dynamic equilibrium enables Ru-based catalysts to facilitate hydrogen shuttling during nitrate reduction efficiently.

To better understand the role of H* in the NO_3^-RR and the reaction pathway of the electrocatalytic process, *in-situ* ATR-SEIRAS was employed to monitor the reaction process. As shown in Fig. 4e-f, with the progress of the reaction, the adsorption capacity of the NO_3^- characteristic peak (1340 cm^{-1}) is enhanced, and the water dissociation (1632 cm^{-1}) is also strengthened, which provides a sufficient source of H* for the reaction. After the successive appearance of deoxygenated intermediates ($*NO_2$, *NO), a significant number of NH-related species are finally formed[37,40,69–73]. The exclusive detection of NH-related vibrations on Ru-Cu_2O/Cu, absent in controls, confirms Ru's bifunctional role in suppressing hydrogen evolution reaction (HER) while promoting *NO hydrogenation. This is further evidenced by accelerated H-supply kinetics and optimized hydrogen-transfer efficiency. Further investigation of the NO_3^-RR pathway using online differential electrochemical mass spectroscopy (DEMS) to analyze reaction intermediates and products. As shown in Fig. S26, the m/z signals corresponding to N, NH, NH_2, NH_3, HNO, NHOH, NH_2OH, NO, and NO_2 detected under specific constant potential polarization. The reaction pathway for nitrate reduction on Ru-Cu_2O/Cu is tentatively deduced as $*NO_3 \rightarrow *NO_2 \rightarrow *NO \rightarrow *N \rightarrow *NH \rightarrow *NH_2 \rightarrow *NH_3$ and $*NO_3 \rightarrow *NO_2 \rightarrow *NO \rightarrow *NOH \rightarrow *NHOH \rightarrow *NH_2OH \rightarrow *NH_3$[74]. These findings collectively demonstrate that Ru incorporation promotes multifaceted hydrogen transfer pathways, substantially enhancing the activity of hydrogen adsorption. This modification provides abundant reactive centers for hydrogen shuttling, thereby optimizing proton-coupled electron transfer efficiency.

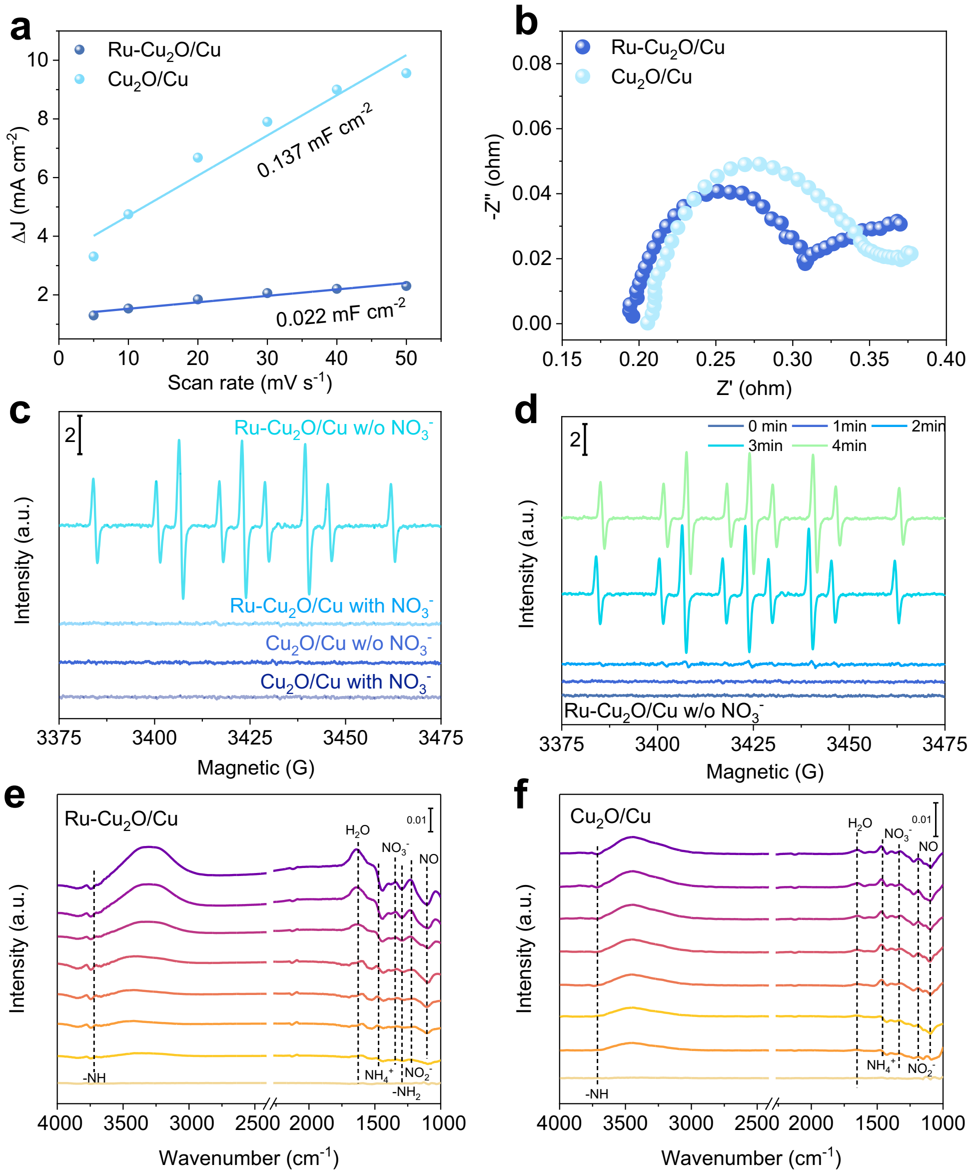

Fig. 4. (a) Relationship between double-layer capacitance and scan rate of Ru-Cu_2O/Cu and Cu_2O/Cu at -0.2 V vs. RHE; (b) EIS of Ru-Cu_2O/Cu and Cu_2O/Cu; (c, d) ESR spectra of DMPO participation of Ru-Cu_2O/Cu and Cu_2O/Cu under different electrolysis conditions; Time-resolved in situ electrochemical ATR-SEIRAS spectra over (e) Ru-Cu_2O/Cu and (f) Cu_2O/Cu at -0.2 V vs. RHE.

To offer a clearer understanding of the reaction pathways on the catalyst surface and the adsorption behavior of intermediate species, the front view of the Ru-Cu_2O/Cu and Cu_2O/Cu computational models is presented in Fig. 5a. The Gibbs free energy for each reaction step was calculated for Ru-Cu_2O/Cu and Cu_2O/Cu, as shown in Fig. 5b-c. It was found that the nitrate active sites on Cu_2O are Cu atoms, while Ru atoms facilitate hydrogen transfer via dual pathways: direct electron donation and H* mediation. This synergistic interplay lowers the overall hydrogenation barrier by 0.30 eV compared to Cu_2O/Cu, thermodynamically favoring multi-step NH_3 synthesis. Critical evaluation of hydrogen adsorption energetics (Fig. 5d) reveals Ru-Cu_2O/Cu achieves a near-optimal ΔG_{H*} of -0.47 eV lower than Cu_2O/Cu (-0.17 eV), demonstrating Ru's unique capability to stabilize H* intermediates[75,76]. The computed reduction in $H^* \rightarrow H_2$ conversion probability directly correlates with experimental FE enhancement, confirming the hydrogen shuttle relay drives efficient eight-electron nitrate-to-ammonia conversion. This enhancement stems from Ru-induced charge redistribution creating electron-rich domains at dual sites, which synergistically optimize $*NO_3^-$ adsorption and proton-coupled electron transfer kinetics. As shown in Fig. 5e and S27, Ru sites establish a hydrogen shuttle highway by first efficiently capturing active hydrogen (H*) from water dissociation, then enabling directional hydrogen transport through electron-enriched Cu_2O domains to nitrate reduction active sites, and ultimately synchronizing hydrogen supply with stepwise nitrate hydrogenation to synergistically drive ammonia synthesis. This process constructs an integrated “trapping-transportation-utilization” hydrogen shuttle highway.

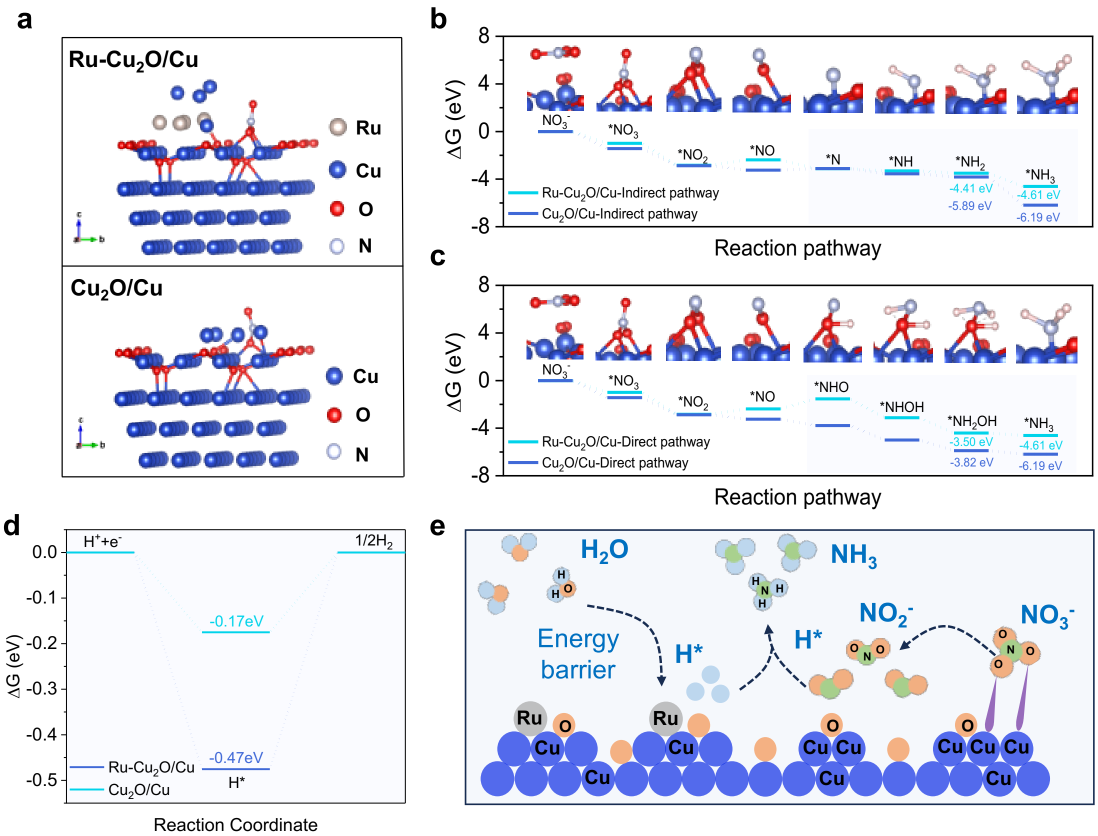

Fig. 5. (a) The front view of the Ru-Cu_2O/Cu and Cu_2O/Cu computational model; (b, c) Free energy of NO_3^-RR on Ru-Cu_2O/Cu and Cu_2O/Cu surface; (d) Gibbs free energy changes for the hydrogen-reduction reaction on Ru-Cu_2O/Cu and Cu_2O/Cu. (e) The reaction pathway for Ru-Cu_2O/Cu in the electrocatalytic NO_3^-RR.

4. Conclusions

In conclusion, this work demonstrates a rationally designed Ru-Cu_2O/Cu catalyst synthesized via stepwise cation exchange, achieving superior nitrate electroreduction performance enabled by an innovative hydrogen shuttle relay mechanism. The introduction of Ru establishes an efficient “hydrogen shuttle relay”, ensuring dynamic matching between the hydrogen supply rate from water dissociation and the hydrogen consumption demand of the nitrate reduction reaction. The optimized catalyst delivers record Faradaic efficiency (95.68%) and NH_3 yield rate (0.82 mmol cm^{-2} h^{-1}) at -0.2 V vs. RHE. Mechanistic studies reveal that Ru incorporation not only induces electron-rich Cu_2O domains but also establishes hydrogen shuttle highways through optimized H* thermodynamics (ΔG_{H*} = -0.47 eV), thereby enabling the synergistic coupling of water dissociation with eight-electron transfer kinetics. The effective matching between hydrogen evolution and consumption ensures enhanced selectivity toward ammonia production from nitrate reduction. These fundamental insights into the hydrogen shuttling mechanism reveal the key pathway for designing high-efficiency dual-site catalysts for sustainable nitrogen cycle engineering.

Credit authorship contribution statement

Heng Guo: Supervision, Conceptualization, Funding acquisition, Project administration, Writing – review and editing. Shiqi Tian: Formal analysis, Investigation, Methodology, Validation, Visualization, Writing – original draft, Writing – review and editing. Shumin Luo: Formal analysis, Methodology, Writing – review and editing. Haoran Wu: Formal analysis, Methodology, Writing – review and editing. Tingsong Li: Formal analysis, Methodology, Writing – review and editing. Guoxing Chen: Formal analysis, Writing – review and editing. Xin Tu: Formal analysis, Writing – review and editing. Weijun Tian: Formal analysis, Writing – review and editing. Chun Tang: Funding acquisition, Writing – review and editing. Guidong Yang: Funding acquisition, Writing – review and editing. Ying Zhou: Supervision, Conceptualization, Funding acquisition, Project administration, Writing – review and editing.

Declaration of Competing Interest

The authors declare that they have no known competing financial interests or personal relationships that could have appeared to influence the work reported in this paper.

Acknowledgements

This work was supported by the National Key R&D project of China (2020YFA0710000), the Provincial International Science and Technology Cooperation Project of Sichuan (2024YFHZ0303), MOHRSS National Foreign Experts Individual

Grant Program (H20240048) and Production-Education Integration Demonstration Project of Sichuan Province “Photovoltaic Industry Production-Education Integration Comprehensive Demonstration Base of Sichuan Province (Sichuan Financial Education [2022] No.106)” and Key Program of Tianfu Yongxing Laboratory (2023KJGG15) provided financial support for this work.

Appendix A. Supplementary material

Supporting Information is available, including additional figures, experimental details, and supplementary data. Supporting Information Available: SEM images of Ru-Cu_2O/Cu, XRD, XPS results, NH_3, NO_2^-, NO_3^- standard curve, DEMS measurements et al.

Data Availability

Data will be made available upon reasonable request.

References

[1] W. Chen, X. Yang, Z. Chen, Z. Ou, J. Hu, Y. Xu, Y. Li, X. Ren, S. Ye, J. Qiu, J. Liu, Q. Zhang, Emerging Applications, Developments, Prospects, and Challenges of Electrochemical Nitrate-to-Ammonia Conversion, Adv. Funct. Mater. 33 (2023) 2300512. https://doi.org/10.1002/adfm.202300512.

[2] K. Chu, B. Weng, Z. Lu, Y. Ding, W. Zhang, R. Tan, Y. Zheng, N. Han, Exploration of Multidimensional Structural Optimization and Regulation Mechanisms: Catalysts and Reaction Environments in Electrochemical Ammonia Synthesis, Adv. Sci. 12 (2025) 2416053. https://doi.org/10.1002/advs.202416053.

[3] Yang X., Han C., Cao Y., He Z., Zhou Y., Recent Advances in Electrocatalytic Nitrate Reduction to Ammonia Using Metal Oxides, J. Inorg. Mater. 39 (2024) 979.

https://doi.org/10.15541/jim20240102.

[4] Q. Wu, W. Zhu, D. Ma, C. Liang, Z. Wang, H. Liang, Screening of transition metal oxides for electrocatalytic nitrate reduction to ammonia at large currents, Nano Res. 17 (2024) 3902–3910. https://doi.org/10.1007/s12274-023-6379-2.

[5] H. Guo, M. Li, Y. Yang, R. Luo, W. Liu, F. Zhang, C. Tang, G. Yang, Y. Zhou, Self-Supported Pd Nanorod Arrays for High-Efficient Nitrate Electroreduction to Ammonia, Small 19 (2023) 2207743. https://doi.org/10.1002/smll.202207743.

[6] T. Li, C. Tang, H. Guo, J. Yang, F. Zhang, G. Yang, Y. Zhou, Understanding first electron transfer kinetic process of electrochemical nitrate reduction to ammonia on Fe_2O_3 nanorods array, Chem. Eng. J. 485 (2024) 149560. https://doi.org/10.1016/j.cej.2024.149560.

[7] Q. Yan, R. Zhao, L. Yu, Z. Zhao, L. Liu, J. Xi, Enhancing Compatibility of Two-Step Tandem Catalytic Nitrate Reduction to Ammonia Over P-Cu/$Co(OH)_2$, Adv. Mater. 36 (2024) 2408680. https://doi.org/10.1002/adma.202408680.

[8] D. Liu, L. Qiao, S. Peng, H. Bai, C. Liu, W.F. Ip, K.H. Lo, H. Liu, K.W. Ng, S. Wang, X. Yang, H. Pan, Recent Advances in Electrocatalysts for Efficient Nitrate Reduction to Ammonia, Adv. Funct. Mater. 33 (2023) 2303480. https://doi.org/10.1002/adfm.202303480.

[9] W. Li, P. Wang, P. Wang, H. Liu, C. Wu, Y. Liu, J. Huang, Z. Fang, H. Guo, Y. Zhang, F. Li, T. Wu, X. Sun, Octahedral CoS_2 electrocatalysts for efficient nitrate reduction to ammonia, Inorg. Chem. Front. 11 (2024) 7118–7125. https://doi.org/10.1039/D4QI01632G.

[10] J. Lv, A. Cao, Y. Zhong, Q. Lin, X. Li, H.B. Wu, J. Yan, A. Wu, Promoting the OH cycle on an activated dynamic interface for electrocatalytic ammonia synthesis, Nat. Commun. 15 (2024) 6675. https://doi.org/10.1038/s41467-024-50988-5.

[11] Y. Bai, Y. Zhang, J. Hu, J. Li, S. Wan, J. Lin, Y. Wang, S. Wang, Hydrogen-Assisted Dissociation of N_2: Prevalence and Consequences for Ammonia Synthesis on Supported Ru Catalysts, ACS Catal. 15 (2025) 1455–1466. https://doi.org/10.1021/acscatal.4c06966.

[12] Y. Yang, Y. Sun, Y. Wang, X. Zhang, W. Zhang, Z.-F. Huang, L. Yin, A. Han, G. Liu, Self-Triggering a Locally Alkaline Microenvironment of Co_4Fe_6 for Highly Efficient Neutral Ammonia Electrosynthesis, J. Am. Chem. Soc. 147 (2025) 8893–8905. https://doi.org/10.1021/jacs.5c00688.
[13] J. Ye, J. Du, A. Wang, Y. Yang, J. Zhu, W. Li, C. Wan, F. Yin, G. He, H. Chen, Reduced spinel oxide $ZnCo_2O_4$ with tetrahedral Co^{2+} sites for electrochemical nitrate reduction to ammonia and energy conversion, Chem. Eng. J. 498 (2024) 155354. https://doi.org/10.1016/j.cej.2024.155354.
[14] K. Zhang, B. Li, F. Guo, N. Graham, W. He, W. Yu, Unveiling the Dual Role of Oxophilic Cr^{4+} in Cr-Cu_2O Nanosheet Arrays for Enhanced Nitrate Electroreduction to Ammonia, Angew. Chem. Int. Ed. 63 (2024) e202411796. https://doi.org/10.1002/anie.202411796.
[15] J. Liu, J. Zhang, H. Deng, S. Wang, X. Jiang, L. Wang, C. Wang, Understanding the activity origin of Pd-anchored single-atom alloy catalysts for NO-to-NH_3 conversion by DFT studies and machine learning, Chin. Chem. Lett. (2024) 110656. https://doi.org/10.1016/j.cclet.2024.110656.
[16] J. Wang, Q. Qin, Z. Wang, X. Zhao, Y. Chen, L. Hou, S. Liu, X. Liu, P-Doped Carbon-Supported $Zn_xP_yO_z$ for Efficient Ammonia Electrosynthesis under Ambient Conditions, Acta Phys.-Chim. Sin. 40 (2024) 2304044. https://doi.org/10.3866/PKU.WHXB202304044.
[17] X. Sun, Y. He, M. Wang, Q. Cheng, Y. Huan, S. Liu, J. Liu, T. Qian, C. Yan, J. Lu, Maximizing Available Active Hydrogen on FeNi Substitutional Solid-Solution Alloy to Boost Electrosynthesis of Ammonia from Nitrate, ACS Nano 19 (2025) 8189–8199. https://doi.org/10.1021/acsnano.4c17163.
[18] Y. Dai, S. Li, X. Li, K. Liu, Y. Guo, H. Li, B. Jiang, Tandem Active Sites in Cu/Mo-WO_3 Electrocatalysts for Efficient Electrocatalytic Nitrate Reduction to Ammonia, Adv. Funct. Mater. (2025) 2420282. https://doi.org/10.1002/adfm.202420282.
[19] W. Gao, K. Xie, J. Xie, X. Wang, H. Zhang, S. Chen, H. Wang, Z. Li, C. Li, Alloying of Cu with Ru Enabling the Relay Catalysis for Reduction of Nitrate to

Ammonia, Adv. Mater. 35 (2023) 2202952. https://doi.org/10.1002/adma.202202952.

[20] X.-H. Wang, Z.-M. Wang, Q.-L. Hong, Z.-N. Zhang, F. Shi, D.-S. Li, S.-N. Li, Y. Chen, Oxygen-Vacancy-Rich Cu_2O Hollow Nanocubes for Nitrate Electroreduction Reaction to Ammonia in a Neutral Electrolyte, Inorg. Chem. 61 (2022) 15678–15685. https://doi.org/10.1021/acs.inorgchem.2c02716.

[21] H. Wang, Q. Mao, T. Ren, T. Zhou, K. Deng, Z. Wang, X. Li, Y. Xu, L. Wang, Synergism of Interfaces and Defects: Cu/Oxygen Vacancy-Rich Cu-Mn_3O_4 Heterostructured Ultrathin Nanosheet Arrays for Selective Nitrate Electroreduction to Ammonia, ACS Appl. Mater. Interfaces 13 (2021) 44733–44741. https://doi.org/10.1021/acsami.1c11249.

[22] A. Feng, Y. Hu, X. Yang, H. Lin, Q. Wang, J. Xu, A. Liu, G. Wu, Q. Li, ZnO Nanowire Arrays Decorated with Cu Nanoparticles for High-Efficiency Nitrate to Ammonia Conversion, ACS Catal. 14 (2024) 5911–5923. https://doi.org/10.1021/acscatal.3c04398.

[23] Y. Wang, A. Xu, Z. Wang, L. Huang, J. Li, F. Li, J. Wicks, M. Luo, D.-H. Nam, C.-S. Tan, Y. Ding, J. Wu, Y. Lum, C.-T. Dinh, D. Sinton, G. Zheng, E.H. Sargent, Enhanced Nitrate-to-Ammonia Activity on Copper–Nickel Alloys via Tuning of Intermediate Adsorption, J. Am. Chem. Soc. 142 (2020) 5702–5708. https://doi.org/10.1021/jacs.9b13347.

[24] Y. Xu, M. Wang, K. Ren, T. Ren, M. Liu, Z. Wang, X. Li, L. Wang, H. Wang, Atomic defects in pothole-rich two-dimensional copper nanoplates triggering enhanced electrocatalytic selective nitrate-to-ammonia transformation, J. Mater. Chem. A 9 (2021) 16411–16417. https://doi.org/10.1039/D1TA04743D.

[25] H. Shi, X.-Y. Sun, S.-P. Zeng, Y. Liu, G.-F. Han, T.-H. Wang, Z. Wen, Q.-R. Fang, X.-Y. Lang, Q. Jiang, Nanoporous Nonprecious High-Entropy Alloys as Multisite Electrocatalysts for Ampere-Level Current-Density Hydrogen Evolution, Small Struct. 4 (2023) 2300042. https://doi.org/10.1002/sstr.202300042.

[26] W. Wan, Y. Zhou, S. Zeng, H. Shi, R. Yao, Z. Wen, X. Lang, Q. Jiang, Nanoporous

Intermetallic Cu_3Sn/Cu Hybrid Electrodes as Efficient Electrocatalysts for Carbon Dioxide Reduction, Small 17 (2021) 2100683. https://doi.org/10.1002/smll.202100683.

[27] H. Shi, Y.-T. Zhou, R.-Q. Yao, W.-B. Wan, X. Ge, W. Zhang, Z. Wen, X.-Y. Lang, W.-T. Zheng, Q. Jiang, Spontaneously separated intermetallic Co_3Mo from nanoporous copper as versatile electrocatalysts for highly efficient water splitting, Nat. Commun. 11 (2020) 2940. https://doi.org/10.1038/s41467-020-16769-6.

[28] J. Wang, B. Guo, J. Sun, Y. Zhou, C. Zhao, Z. Wei, J. Guo, Cooperative hydrogen evolution reaction combining $Cu_{2+1}O$ and Ru active sites, Appl. Catal. B Environ. 324 (2023) 122169. https://doi.org/10.1016/j.apcatb.2022.122169.

[29] X. Zhao, Q. Geng, F. Dong, K. Zhao, S. Chen, H. Yu, X. Quan, Boosting the selectivity and efficiency of nitrate reduction to ammonia with a single-atom Cu electrocatalyst, Chem. Eng. J. 466 (2023) 143314. https://doi.org/10.1016/j.cej.2023.143314.

[30] B. Zhou, Y. Tong, Y. Yao, W. Zhang, G. Zhan, Q. Zheng, W. Hou, X.-K. Gu, L. Zhang, Reversed I_1Cu_4 single-atom sites for superior neutral ammonia electrosynthesis with nitrate, Proc. Natl. Acad. Sci. U.S.A. 121 (2024) e2405236121. https://doi.org/10.1073/pnas.2405236121.

[31] Y.-C. Zhang, M. Zhao, J. Wu, Y. Wang, L. Zheng, F. Gu, J.-J. Zou, J. Gao, X.-D. Zhu, Construction of Pt Single-Atom and Cluster/FeOOH Synergistic Active Sites for Efficient Electrocatalytic Hydrogen Evolution Reaction, ACS Catal. 14 (2024) 7867–7876. https://doi.org/10.1021/acscatal.4c01133.

[32] W. Qiu, M. Xie, P. Wang, T. Gao, R. Li, D. Xiao, Z. Jin, P. Li, Size-Defined Ru Nanoclusters Supported by TiO_2 Nanotubes Enable Low-Concentration Nitrate Electroreduction to Ammonia with Suppressed Hydrogen Evolution, Small 19 (2023) 2300437. https://doi.org/10.1002/smll.202300437.

[33] Q. Wu, X. Fan, K. Liu, X. Quan, Y. Liu, Efficient and selective electroreduction of nitrate to ammonia via interfacial engineering of B-doped Cu nanoneedles, Appl. Catal. B Environ. 361 (2025) 124597.

https://doi.org/10.1016/j.apcatb.2024.124597.
[34] Y. Yu, Y. Cheng, S. Cheng, Z. Wu, Advanced Ruthenium-Based Electrocatalysts for NO_x Reduction to Ammonia, Adv. Mater. 37 (2025) 2412363. https://doi.org/10.1002/adma.202412363.
[35] J.-J. Zhang, Y.-Y. Lou, Z. Wu, X.J. Huang, S.-G. Sun, Spatially Separated Cu/Ru on Ordered Mesoporous Carbon for Superior Ammonia Electrosynthesis from Nitrate over a Wide Potential Window, J. Am. Chem. Soc. 146 (2024) 24966–24977. https://doi.org/10.1021/jacs.4c06657.
[36] J. Wang, C. He, J. Huo, L. Fu, C. Zhao, A Theoretical Evaluation of Possible N_2 Reduction Mechanism on Mo_2B_2, Adv. Theory Simul. 4 (2021) 2100003. https://doi.org/10.1002/adts.202100003.
[37] Y. Zheng, Y. Jiao, A. Vasileff, S. Qiao, The Hydrogen Evolution Reaction in Alkaline Solution: From Theory, Single Crystal Models, to Practical Electrocatalysts, Angew. Chem. Int. Ed. 57 (2018) 7568–7579. https://doi.org/10.1002/anie.201710556.
[38] X. Zhang, L. Liu, J. Feng, X. Ju, J. Wang, T. He, P. Chen, Ru Nanoparticles on Pr_2O_3 as an Efficient Catalyst for Hydrogen Production from Ammonia Decomposition, Catal. Lett. 152 (2022) 1170–1181. https://doi.org/10.1007/s10562-021-03709-2.
[39] Q. Fang, Z. Zhang, X. Yang, T. Cheng, X. Ma, J. Tang, Cu_2O Nanoparticles with Controlled Surface Roughness for CO_2 Electroreduction Towards C_{2+} Products, Chem. Eng. J. 515 (2025) 163293. https://doi.org/10.2139/ssrn.5076344.
[40] Q. Hu, K. Yang, O. Peng, M. Li, L. Ma, S. Huang, Y. Du, Z.-X. Xu, Q. Wang, Z. Chen, M. Yang, K.P. Loh, Ammonia Electrosynthesis from Nitrate Using a Ruthenium–Copper Cocatalyst System: A Full Concentration Range Study, J. Am. Chem. Soc. 146 (2024) 668–676. https://doi.org/10.1021/jacs.3c10516.
[41] W. Yang, H. Liu, X. Chang, Y. Zhang, Y. Cai, Y. Li, Y. Cui, B. Xu, L. Yu, X. Cui, D. Deng, Electrosynthesis of NH_3 from NO with ampere-level current density in a pressurized electrolyzer, Nat. Commun. 16 (2025) 1257.

https://doi.org/10.1038/s41467-025-56548-9.

[42] L. Sun, X. Min, J. Wang, Y. Yang, S. Han, D. Fan, Y. Jing, D. Xu, W. Wang, B. Liu, Enabling High Performance in a Positive Potential of Nitrate-to-Ammonia Electrocatalysis Over Mesoporous Core@Shell Cu_2O/Cu@PdCu Nanozyme, Adv. Mater. (2025) 2503291. https://doi.org/10.1002/adma.202503291.

[43] S. Luo, H. Guo, T. Li, H. Wu, F. Zhang, C. Tang, G. Chen, G. Yang, Y. Zhou, Ruthenium-induced hydrolysis effect on Fe_2O_3 nanoarrays for high-performance electrochemical nitrate reduction to ammonia, Appl. Catal. B Environ. 351 (2024) 123967. https://doi.org/10.1016/j.apcatb.2024.123967.

[44] J. Zhao, Y. Yuan, F. Zhao, W. Han, Q. Yuan, M. Kou, J. Zhao, C. Chen, S. Wang, Identifying the facet-dependent active sites of Cu_2O for selective C-N coupling toward electrocatalytic urea synthesis, Appl. Catal. B Environ. 340 (2024) 123265. https://doi.org/10.1016/j.apcatb.2023.123265.

[45] X. Liu, Y. Wang, Z. Hu, B. Yang, R.L. Smith, Y. Su, X. Qi, Self-reducing Cu_2O/Cu nanosheet interface for efficient electrocatalytic production of ammonium from nitrate, Appl. Catal. B Environ. 371 (2025) 125254. https://doi.org/10.1016/j.apcatb.2025.125254.

[46] S. Liu, L. Cui, S. Yin, H. Ren, Z. Wang, Y. Xu, X. Li, L. Wang, H. Wang, Heterointerface-triggered electronic structure reformation: Pd/CuO nano-olives motivate nitrite electroreduction to ammonia, Appl. Catal. B Environ. 319 (2022) 121876. https://doi.org/10.1016/j.apcatb.2022.121876.

[47] Z. Chen, Y. Zhao, H. Huang, G. Liu, H. Zhang, Y. Yan, H. Li, L. Liu, M. Liu, D. Wang, J. Zeng, Isolated Copper Atoms Boost *NO_3 Adsorption and Active Hydrogen Retention over Zinc Oxide for Ammonia Electrosynthesis at Ampere-Level Current Densities, J. Am. Chem. Soc. 147 (2025) 18737–18746. https://doi.org/10.1021/jacs.5c01863.

[48] Y. Hua, N. Song, Z. Wu, Y. Lan, H. Luo, Q. Song, J. Yang, Cu–Fe Synergistic Active Sites Boost Kinetics of Electrochemical Nitrate Reduction, Adv. Funct. Mater. 34 (2024) 2314461. https://doi.org/10.1002/adfm.202314461.

[49] Y. Zheng, Y. Jia, Q. Cao, L. Li, X. Yu, S. Zeng, H. Yao, X. Guo, In situ evolution of Sn/Cu_2O heterostructure catalysts for modulating selectivity in electrosynthesis of ammonia and urea, Nano Res. 18 (2025) 94907248. https://doi.org/10.26599/NR.2025.94907248.

[50] Z. Yao, S. Liu, H. Liu, Y. Ruan, S. Hong, T. Wu, L. Hao, Y. Soo, P. Xiong, M.M. Li, A.W. Robertson, Q. Xia, L. Ding, Z. Sun, Pre-Adsorbed H-Assisted N_2 Activation on Single-Atom Cadmium-O_5 Decorated In_2O_3 for Efficient NH_3 Electrosynthesis, Adv. Funct. Mater. 33 (2023) 2209843. https://doi.org/10.1002/adfm.202209843.

[51] Y. Yang, D. Pang, C. Wang, Z. Fu, N. Liu, J. Liu, H. Wu, B. Jia, Z. Guo, X. Fan, J. Zheng, Vacancy and Dopant Co-Constructed Active Microregion in Ru-MoO_{3-x}/Mo_2AlB_2 for Enhanced Acidic Hydrogen Evolution, Angew. Chem. Int. Ed. (2025) e202504084. https://doi.org/10.1002/anie.202504084.

[52] X. Ren, M. Li, K. Wang, R. Lu, M. Lu, P. Li, Y. Yao, S. Jin, Z. Wang, S. Tian, Enhanced Tri-Atom Ru-Based Catalyst for Hydrogen Evolution Reaction via Rapid Pyrolysis of Precursor, Adv. Funct. Mater. (2025) 2503678. https://doi.org/10.1002/adfm.202503678.

[53] H. Guo, Z. Guo, G. Xue, H. Wang, J. Gong, K. Chu, J. Qin, Y. Guan, H. Dong, Y. Chen, Y. Miao, C. Zhang, H. Liu, T. Liu, J. Hofkens, F. Lai, Entropy-Driven Stabilization of Noble Metal Single Atoms: Advancing Ammonia Synthesis and Energy Output in Zinc-Nitrate Batteries, Adv. Mater. 37 (2025) 2500224. https://doi.org/10.1002/adma.202500224.

[54] X. Liu, C. Xu, X. Chen, J. Liu, F. Jiang, X. Cheng, Q. Xu, J. Lu, Modulation of Cu Electronic Structure to Accelerate the Conversion of Key Intermediates for Electrocatalytic Ammonia Synthesis, ACS Catal. (2025) 6141–6149. https://doi.org/10.1021/acscatal.4c07167.

[55] J. Dong, X. Song, Y. Chen, Z. Gai, Z. Yuan, D. Liu, Z. Tan, A. Liu, X. Wang, S. Song, Engineering Ce Promoter to Regulate H^* Species to Boost Tandem Electrocatalytic Nitrate Reduction for Ammonia Synthesis, Adv. Funct. Mater.

(2025) 2422025. https://doi.org/10.1002/adfm.202422025.

[56] Q. Gao, H.S. Pillai, Y. Huang, S. Liu, Q. Mu, X. Han, Z. Yan, H. Zhou, Q. He, H. Xin, H. Zhu, Breaking adsorption-energy scaling limitations of electrocatalytic nitrate reduction on intermetallic CuPd nanocubes by machine-learned insights, Nat. Commun. 13 (2022) 2338. https://doi.org/10.1038/s41467-022-29926-w.

[57] S. Li, J. Yan, M. Liu, H. Su, Localized enriching nitrate/proton on reconstituted Fe nanoparticles boosting electrocatalytic nitrate reduction to ammonia, J. Energy Chem. 103 (2025) 682–691. https://doi.org/10.1016/j.jechem.2024.12.011.

[58] S. Zhang, J. Wu, M. Zheng, X. Jin, Z. Shen, Z. Li, Y. Wang, Q. Wang, X. Wang, H. Wei, J. Zhang, P. Wang, S. Zhang, L. Yu, L. Dong, Q. Zhu, H. Zhang, J. Lu, Fe/Cu diatomic catalysts for electrochemical nitrate reduction to ammonia, Nat. Commun. 14 (2023) 3634. https://doi.org/10.1038/s41467-023-39366-9.

[59] W. Yang, Z. Chang, X. Yu, R. Shen, L. Wang, X. Cui, J. Shi, Triple Regulations via Fe Redox Boosting Nitrate Reduction to Ammonia at Industrial Current Densities, Angew. Chem. Int. Ed. 64 (2025) e202415300. https://doi.org/10.1002/anie.202415300.

[60] H. Zhu, Y. Tang, J.J. Wang, T. Sun, M. Wang, J. Wang, Y. Tan, J. Wang, Accelerating electrosynthesis of ammonia from nitrates using coupled NiO/Cu nanocomposites, Chem. Commun. 60 (2024) 2184–2187. https://doi.org/10.1039/D3CC05928F.

[61] K. Liu, Z. Sun, X. Peng, X. Liu, X. Zhang, B. Zhou, K. Yu, Z. Chen, Q. Zhou, F. Zhang, Y. Wang, X. Gao, W. Chen, P. Chen, Tailoring asymmetric RuCu dual-atom electrocatalyst toward ammonia synthesis from nitrate, Nat. Commun. 16 (2025) 2167. https://doi.org/10.1038/s41467-025-57463-9.

[62] H. Wang, S. Man, H. Wang, V. Presser, Q. Yan, Y. Zhang, Grave-to-cradle upcycling of harmful algal biomass into atomically dispersed iron catalyst for efficient ammonia electrosynthesis from nitrate, Appl. Catal. B Environ. 332 (2023) 122778. https://doi.org/10.1016/j.apcatb.2023.122778.

[63] H. Guo, P. Yang, Y. Yang, H. Wu, F. Zhang, Z. Huang, G. Yang, Y. Zhou, Vacancy-

Mediated Control of Local Electronic Structure for High-Efficiency Electrocatalytic Conversion of N_2 to NH_3, Small 20 (2024) 2309007. https://doi.org/10.1002/smll.202309007.

[64] Y. Li, J. Ma, Z. Wu, Z. Wang, Direct Electron Transfer Coordinated by Oxygen Vacancies Boosts Selective Nitrate Reduction to N_2 on a Co–CuO_x Electroactive Filter, Environ. Sci. Technol. 56 (2022) 8673–8681. https://doi.org/10.1021/acs.est.1c05841.

[65] X. Lu, J. Yu, J. Cai, Q. Zhang, S. Yang, L. Gu, G.I.N. Waterhouse, S.-Q. Zang, B. Yang, S. Lu, Exclusive nitrate to ammonia conversion via boron-doped carbon dots induced surface Lewis acid sites, Cell Rep. Phys. Sci. 3 (2022) 100961. https://doi.org/10.1016/j.xcrp.2022.100961.

[66] Y. Ren, F. Tian, L. Jin, Y. Wang, J. Yang, S. You, Y. Liu, Fluidic MXene Electrode Functionalized with Iron Single Atoms for Selective Electrocatalytic Nitrate Transformation to Ammonia, Environ. Sci. Technol. 57 (2023) 10458–10466. https://doi.org/10.1021/acs.est.3c02520.

[67] G. Zhang, X. Li, K. Chen, Y. Guo, D. Ma, K. Chu, Tandem Electrocatalytic Nitrate Reduction to Ammonia on MBenes, Angew. Chem. Int. Ed. 62 (2023) e202300054. https://doi.org/10.1002/anie.202300054.

[68] R. Ge, Y. Wang, Z. Li, M. Xu, S. Xu, H. Zhou, K. Ji, F. Chen, J. Zhou, H. Duan, Selective Electrooxidation of Biomass-Derived Alcohols to Aldehydes in a Neutral Medium: Promoted Water Dissociation over a Nickel-Oxide-Supported Ruthenium Single-Atom Catalyst, Angew. Chem. 134 (2022) e202200211. https://doi.org/10.1002/ange.202200211.

[69] W. Liu, J. Chen, Y. Wei, Y. He, Y. Huang, M. Wei, Y. Yu, N. Yang, W. Zhang, L. Zhang, F. Saleem, F. Huo, Regulating Local Electron Distribution of Cu Electrocatalyst via Boron Doping for Boosting Rapid Absorption and Conversion of Nitrate to Ammonia, Adv. Funct. Mater. 34 (2024) 2408732. https://doi.org/10.1002/adfm.202408732.

[70] X. Fan, Z. Teng, L. Han, Y. Shen, X. Wang, W. Qu, J. Song, Z. Wang, H. Duan,

Y.A. Wu, B. Liu, D. Zhang, Boosted charge and proton transfer over ternary $Co/Co_3O_4/CoB$ for electrochemical nitric oxide reduction to ammonia, Nat. Commun. 16 (2025) 4874. https://doi.org/10.1038/s41467-025-60043-6.

[71] W. Liu, M. Xia, C. Zhao, B. Chong, J. Chen, H. Li, H. Ou, G. Yang, Efficient ammonia synthesis from the air using tandem non-thermal plasma and electrocatalysis at ambient conditions, Nat. Commun. 15 (2024) 3524. https://doi.org/10.1038/s41467-024-47765-9.

[72] L. Yang, C. Wang, Y. Li, W. Ge, L. Tang, J. Shen, Y. Zhu, C. Li, Frustrated Lewis Pairs on Zr Single Atoms Supported N-Doped TiO_{2-x} Catalysts for Electrochemical Nitrate Reduction To Ammonia, Adv. Funct. Mater. 34 (2024) 2401094. https://doi.org/10.1002/adfm.202401094.

[73] Y. Wang, Y. Xu, C. Cheng, B. Zhang, B. Zhang, Y. Yu, Phase-Regulated Active Hydrogen Behavior on Molybdenum Disulfide for Electrochemical Nitrate-to-Ammonia Conversion, Angew. Chem. Int. Ed. 63 (2024) e202315109. https://doi.org/10.1002/anie.202315109.

[74] W. Yang, Z. Chang, X. Yu, P. Wu, R. Shen, L. Wang, X. Cui, J. Shi, Cu-Co Dual Sites Tandem Synergistic Effect Boosting Neutral Low Concentration Nitrate Electroreduction to Ammonia, Adv. Sci. 12 (2025) 2416386. https://doi.org/10.1002/advs.202416386.

[75] H. Li, X. Zhao, H. Liu, S. Chen, X. Yang, C. Lv, H. Zhang, X. She, D. Yang, Sub-1.5 nm Ultrathin CoP Nanosheet Aerogel: Efficient Electrocatalyst for Hydrogen Evolution Reaction at All pH Values, Small 14 (2018) 1802824. https://doi.org/10.1002/smll.201802824.

[76] J. Liu, G. Ding, J. Yu, X. Liu, X. Zhang, J. Guo, J. Zhang, W. Ren, R. Che, Visualizing spatial potential and charge distribution in Ru/N-doped carbon electrocatalysts for superior hydrogen evolution reaction, J. Mater. Chem. A 7 (2019) 18072–18080. https://doi.org/10.1039/C9TA06206H.